Chemical Engineering Science 280 (2023) 118948

Contents lists available at ScienceDirect

Chemical Engineering Science

journal homepage: www.elsevier.com/locate/ces

Remote microwave heating and ignition with an embedded receiving antenna within nanocomposites

Keren Shi, Yujie Wang, Feiyu Xu, Michael R. Zachariah *

University of California, Riverside, CA 92521, USA

ARTICLE INFO

Keywords:
Microwave
Remote ignition
Nanothermites
Antenna

ABSTRACT

This study demonstrates the use of a receiving antenna within a material to transmit microwave energy resulting in dielectric heating and ignition in a direct writing process. The wire antennas themselves do not heat, but rather the induced electric field results in dielectric heating of the sample, and with sufficient electric field strength, triggers ignition. With different length of embedded receiving antenna, local hot spots were generated at the ends of the receiving antenna as imaged with an IR camera. Simulation of a monopole source and receiving antennas, shows a spatial correspondence of the calculated electric field and the measured hot spots. We also demonstrate that receiving antennas can be incorporated to trigger ignition at desired locations, with multiple ignition points from which flame propagations can be induced. This study provides a new way to design and remote control the location of the hot spots and ignition.

1. Introduction.

Ignition is typically a localized phenomenon which ultimately leads to flame propagation and spread (Field, 1992; Granier and Pantoya, 2004; Williams et al., 2012). One of the interesting issues to consider is how one can trigger ignition at a specified location in an energetic material remotely or perhaps in multiple locations so as to induce a predesigned flame spread in both space and time. Microwaves (MW) offer this potential opportunity since most components comprising energetic material are effectively MW transparent (Vargas et al., 2016; Crane et al., 2014). This means that one can, at least in principle, embed absorbing material at specified location so as to initiate ignition or augment combustion.

This concept was demonstrated on a class of metastable intermolecular composites (MICs) that offer significantly higher energy density and a tunable energy release rate as compared to traditional organic chemical energetic systems (Asay et al., 2004). These are typically a composite of metallic fuel (Al, Ti or Mg) and an oxidizer (CuO, Fe_2O_3 or MnO_2), for which rapid and highly exothermic reaction is initiated at the ignition temperature. The energy release rate of a nanothermite system can be tuned by composition, particle diameter and packing density. And the use of components at the nano scale, greatly increases reactivity due to smaller diffusion lengths (Wang et al., 2014).

Prior work has shown that certain reactive MW sensitizers can be used to initiate combustion in nanothermites (Alibay et al., 2021; Kline et al., 2020). Kline et al. showed that the oxidizing shell (mainly TiO_2 and TiN) of nano titanium (nTi) can be dielectric heated to ignite Ti/PVDF thin film and subsequently ignite neighboring layers of non-MW sensitive energetics (Al/PVDF) (Kline et al., 2020). This was theoretically demonstrated by Mie theory calculation by Biswas et al., for coated spheres showing that the optical properties of the delectric coating is key to MW absorption efficiency and heating (Biswas et al., 2020). Al/MnO_x can also be ignited by microwave stimulation by the presence of MnO_2 and Mn_2O_3 as a means to ignite an Al based fuel (Alibay et al., 2022). Barkley et al. studied the role of reduced graphene oxide (rGO) which is a good microwave sensitizer for the Al/Fe_2O_3 system and was able to show ignition in hundreds of milliseconds (Barkley et al., 2021). Cheng et al. doped Al/CuO with microwave absorbing layered Ti_3C_2 to show a significant decrease in ignition delay relative to the undoped sample (Cheng et al., 2022). The key point is that in all these studies, samples were placed either below the microwave probe or within a MW waveguide.

Here we show that embedding a MW receiving antenna within printed energetic composites results in focusing of MW energy at the terminals of the receiving antenna. The focused MW energy further leads to sufficient heating in non-MW sensitive nanothermites, and can induce ignition remotely. The heating rate of the samples was observed by infrared imaging, and investigated with respect to the geometry, length

* Corresponding author at: Department of Chemical and Environmental Engineering, University of California, Riverside, California 92521, USA.
E-mail address: mrz@engr.ucr.edu (M.R. Zachariah).

https://doi.org/10.1016/j.ces.2023.118948
Received 7 February 2023; Received in revised form 12 May 2023; Accepted 28 May 2023
Available online 1 June 2023

of the receiving antenna and power of the source MW antenna. COMSOL simulation of the receiving and source antenna shows that large electric field gradients are generated at both ends of the embedded receiving antenna, which leads to hot-spots in Al/CuO sticks, and induces ignition leading to combustion propagation.

This paper demonstrates that by embedding a metal wire within a poor microwave absorbing system, localized heating and remote ignition can be achieved. The heating rate of the sample is related to the electric field intensity extracted from simulation in this complex electric field environment.

2. Experimental section

2.1. Materials

Aluminum nanoparticles (Al NPs, 80 nm) were purchased from Novacentrix Inc. with an active content of 67 wt% measured by thermogravimetric analysis. Copper oxide (CuO) nanoparticles (40 nm) were purchased from U.S. Research Nanomaterials. METHOCEL^{TM} F4M hydroxypropyl methylcellulose (HPMC) was purchased from Dow Chemical Co. Poly(vinylidene fluoride) (PVDF, average molecular weight ~534000) and N, N-dimethylformamide (DMF) were obtained from Sigma-Aldrich. Aluminum 1199 wire (diameter 0.003 in., ~75 μm) was purchased from California Fina Wire Co. All materials were used as received.

2.2. Sample preparation and fabrication

High loading Al/CuO ink was formulated for a direct writing process, which is detailed in our previous paper (Wang et al., 2021). Al wires were chosen as the receiving antenna to minimize the magnetic field induced under MW. As such the receiving antenna (as will be deomstrated) is not itself heated by MW irradiation, but induces an electric field to heat the nanocomposites. To embed the receiving antenna into the sample, different lengths of Al wires: 5 mm (~1/24λ), 10 mm (~1/12λ), 15 mm (~1/8λ), 20 mm (~1/6λ) and 30 mm (~1/4λ) were placed on top of the 10th printed layer. Then an additional 5 layers were printed. After drying the printed samples was cut into uniform 30 mm (~1/4λ) sticks. Fig. 1**b** shows the SEM image of the cross-section of the Al/CuO stick and embedded receiving antenna.

2.3. Microwave antenna configuration and characterization

A custom monopole MW source antenna was constructed to deliver energy to the receiving antenna remotely. The MW source antenna (**Figure S1**) was connected to a magnetron system (MKS Instruments Inc.) operating at 2.45 GHz (λ = 122.45 mm). The magnetron (MW head TM012) was powered by a switching power supply (SM445), connected to an isolator (VHU210 3 kW), triple-stub tuner (AG340M3) and a dual directional coupler (DC2340N) with a linear power sensor (RD8400) in series. A WR340 cavity to coaxial transition adaptor (Microwave Techniques LLC) was attached at the end of the system. The source antenna was made from 2% thiorated tungsten (diameter: 1 mm, length: ~30 mm, ~1/4λ) and connected to the adaptor by a coaxial cable (Pasternack, LMR400, maximum continuous power: 330 W at 2.45 GHz).

The actual power delivered to the source antenna, and the S_{11} parameter (the reflected power from the source antenna) were measured by a vector network analyzer (VNA, Keysight N9918A) from 2.2 to 2.7 GHz. To measure the power delivery, the source antenna was removed from the coaxial cable, and connected to a 50 dB attenuator (Fairview Microwave, SA3NFF300W-50) then to the VNA. The total external attenuation is −50.6 dB considering the loss at the connection cable.

2.4. Experiment setup and imaging system

All samples were placed 15 mm below the source antenna (Fig. 1**a**). The left end of the samples was placed right under the source antenna tip.

To understand how remote heating was taking place, an infrared (IR) camera (Telops, FAST M3K) was used to measure the surface temperature of the samples at 100–5000 frames per second. A 50 mm lens was coupled with a 0.5-inch extension ring with an exposure time of 5 μs. The resolution of acquired images was 140 μm per pixel, and the measured temperature range used in the experiment was 0–150 °C. A high-speed color camera (Vision Research Phantom, Miro M110) was used to determine the ignition delay of the sample. The exposure time was 24 μs and recorded at 5000 frames per second.

2.5. Heating rate and ignition delay measurement

The IR camera, color camera, and the magnetron system were set to trigger simultaneously. The rise time of the magnetron is 80 ms, and this time delay was subtracted in all measurements. The heating rate was calculated as the temperature increase over a time interval from the IR camera. Ignition was defined as the point of the first light in the color camera **video**. All measurements were repeated in triplicate unless otherwise stated.

2.6. Source and receiving antenna simulation

Simulation of the interaction between source and receiving antenna was performed in COMSOL Multiphysics 5.6. The frequency of the source antenna was 2.45 GHz and the input power was set to be 76, 153, 222 W. Al and CuO nano particles and polymer matrix were not

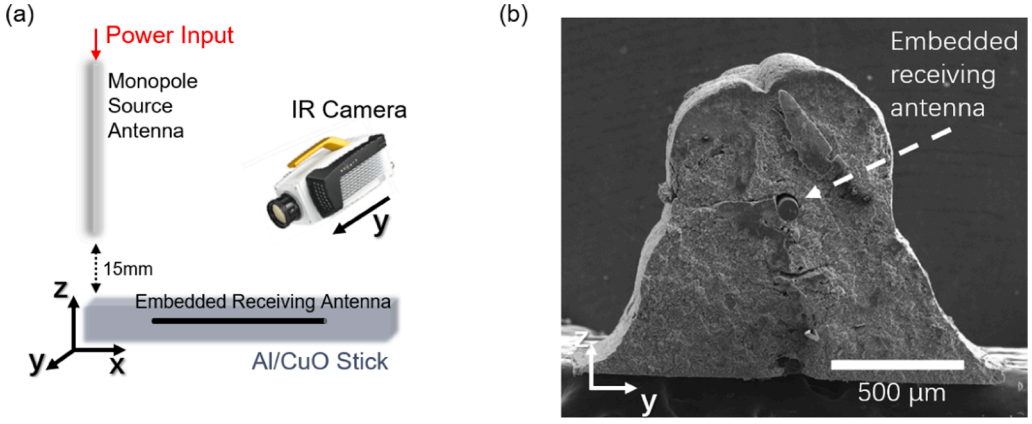

Fig. 1. (a) Diagram of the experiment setup. The samples were placed 15 mm below the monopole source antenna. (b) SEM image of the cross-section of the Al/CuO stick and embedded receiving antenna (Al wire). The cross-section area is ~1 mm^2.

explicitly include in the model (**Figure S2**). The parameters of tungsten and aluminum were from the COMSOL build-in material properties.

3. Results and discussion

3.1. High power microwave antenna characterization

To understand the power coupling between the magnetron and the custom monopole antenna through the WR340 transition adapter, a VNA was connected to the adaptor and used to measure the channel power between 2.2 and 2.7 GHz. Fig. 2**a** shows the relationship between the power delivered to the source antenna and the magnetron output power. At the lower power range (<150 W), almost 100% of the output power was delivered to the source antenna. However, with increasing magnetron output power, the conversion rate dropped to ~ 65%. This implies that the power loss at the WR340 adaptor and the coaxial cable is increasing at the high-power range. To keep the source antenna operating at a constant power, the magnetron output power was kept below 330 W. The overall conversion rate of the WR340 adaptor is ~ 68% in this power range. For the subsequent heating experiments, three power levels which delivered to the source antenna were used, 76 W (minimum operational power), 153 W and 222 W (maximum operational power).

To better understand the performance of the source antenna, a monopole antenna simulation was done with COMSOL. Fig. 2**b** shows the simulated S_{11} parameter which represents how much power is reflected from the antenna, for a 1/4λ monopole antenna, along with the measurement from the VNA. The simulation results show that the monopole source antenna has a minimum reflection of −12.5 dB at 2.45 GHz. The VNA measurement agrees quite well with the simulation. The measured S_{11} parameter at 2.45 GHz was ~ -14 dB, indicating that only 4% of energy is reflected back by the source antenna.

3.2. Role of embedded receiving antenna

We begin by noting that the printed Al/CuO sample itself shows no obvious heating effect under microwave irradiation when placed remotely (15 mm below the source antenna) at all power levels (Fig. 3**a and Figure S3**) in the absence of the receiving antenna. This can be attributed to the low relativity permittivity (ε = ε' - i ε'') of the Al and CuO nano particles and low electric field intensity when the source antenna is 15 mm away from sample. The relative permittivity of the Al/CuO nano particles (equivalence ratio, φ = 1) is 3.3 – 0.25i (Cheng et al., 2022). The simulation confirms the experimental observation, showing that the average electric field intensity is only 4000 V/m 15 mm below the source antenna (at sample position), which is insufficient to achieve any significant heating **(dash line in** Fig. 3**c and Figure S4)**.

However, incorporation of the receiving antenna (length, L = 1/8λ) within the Al/CuO sample results in two hot spots (Fig. 3**b**). *It is important to note at this point that the microwave is not heating the receiving antenna.* This was checked by using an Al wire at the same location in the absence of the sample and monitoring heating with the IR camera. This control experiment indicates that the hot spots are not generated by heat transfer from the embedded receiving antenna (Al wire) to Al/CuO nano particles. Since both Al and CuO are non-magnetic, the main heating mechanism would be dielectric loss generated by the Al/CuO nano particles (Wang et al., 2012; Himmetoglu et al., 2011). To better understand this effect with the embedded receiving antenna, a simulation of the monopole source antenna and the receiving antenna (Al wire) was conducted with COMSOL. The results (Fig. 3**c**) show that the embedded Al wire works as a receiving antenna within the sample, and large electric field gradients are induced at both ends of the receiving antenna, with a peak electric field intensity ~ 20x higher compared to the case without the receiving antenna. This is a direct indication that a receiving antenna can be used for location control and amplification of heating.

Fig. 3**(d)** plots the temporal temperature profile of the two hot spots generated at the ends of the receiving antenna. Overall the temperature profile shows that the heating rates of both hot spots gradually decreasing with time until they reach a steady state. To better understand the thermal response of the sample with the receiving antenna, this temperature profile was divided into three regions.

In the first linear heating region, the relative permittivity and specific heat capacity of the Al/CuO nano particles are assumed to be constant. The linear heating rates of the two hot spots can be calculated in this region **(solid line in** Fig. 3**e)**. The heating rate of materials under microwave stimulation is proportion to the square of the electric field intensity. Under the assumption of negligible heat loss and neglection of thermal diffusion (a poor assumption in general) the heating rate can be expressed as (Gabriel et al., 1998):

$$\frac{\Delta T}{t} = \frac{\omega \varepsilon_0 \varepsilon' tan\delta}{\rho C} |E|^2 \tag{1}$$

where $\omega = 2\pi f$ is the angular frequency, ε_0 is the vacuum permittivity, ε' and $tan\delta$ are the real part of the relative permittivity and the loss tangent, ρ is density, C is the specific heat capacity. Electric field intensity (|E|) is the average electric field in the 0.5 × 0.5 × 0.5 mm region centered at the two terminals of the receiving antenna.

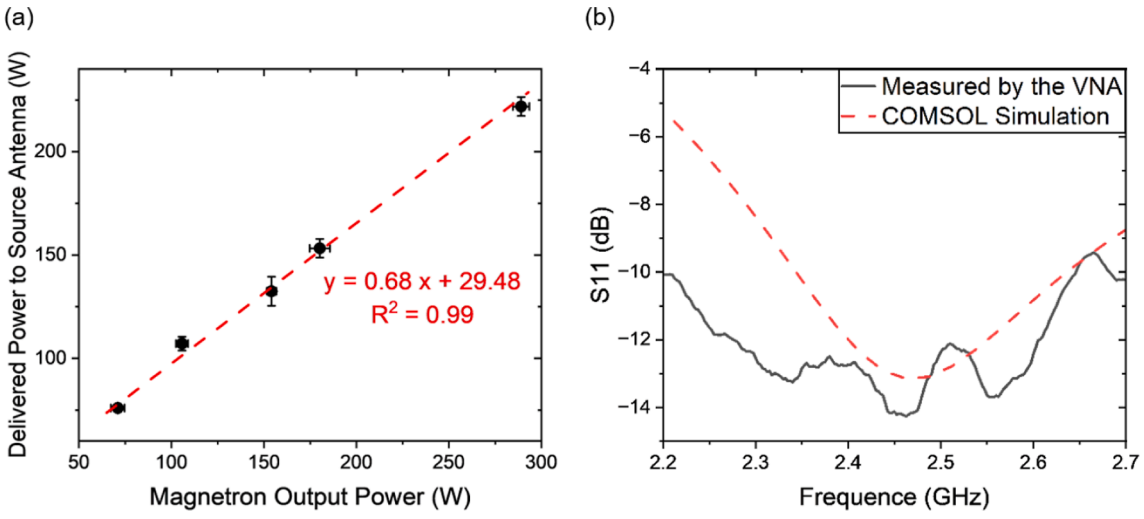

Fig. 2. (a) Power delivered to the source antenna measured by the VNA (y-axis), and the magnetron output power (x-axis). (b) Measured and simulated S_{11} parameter of the monopole source antenna.

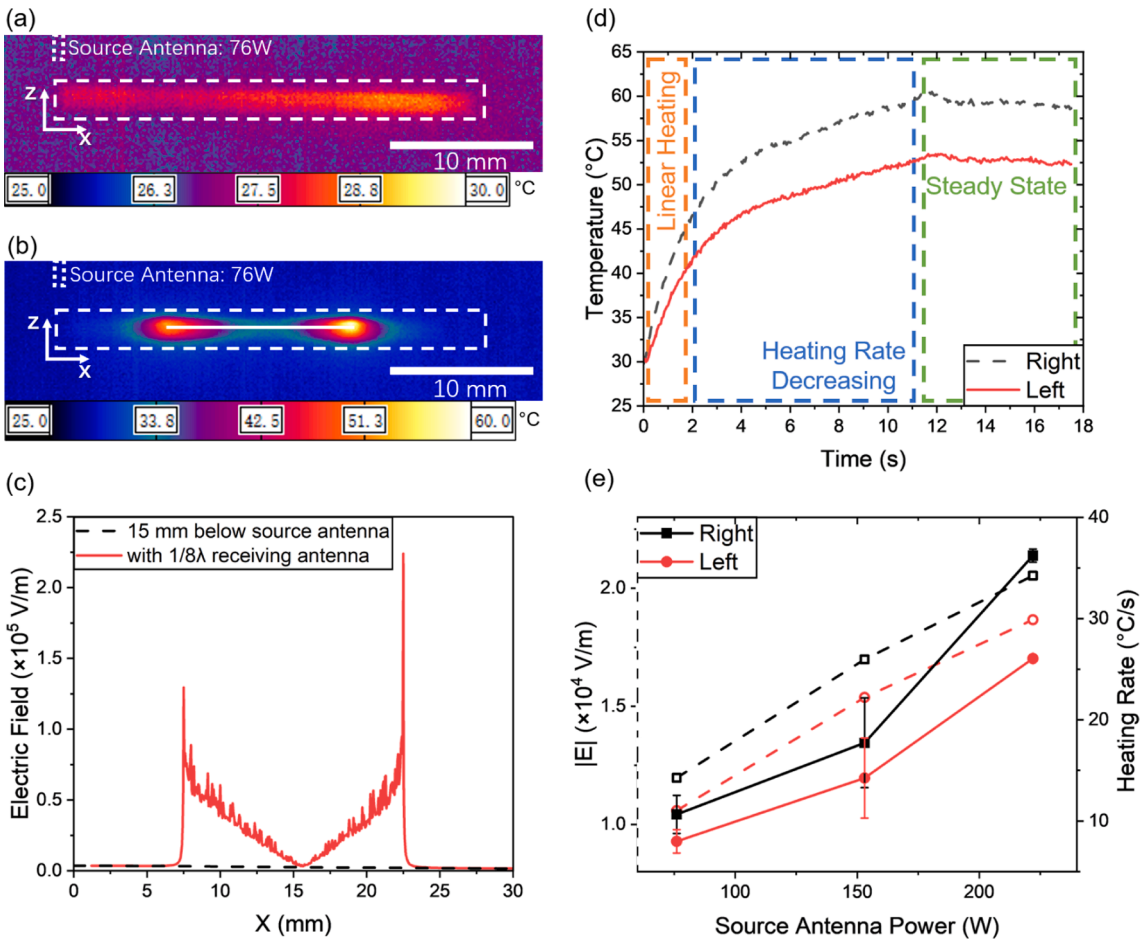

Fig. 3. (a) IR image of the Al/CuO sample **without** embedding receiving antenna at steady state (sample placed 15 mm below source antenna). (b) IR image of the Al/CuO sample **with** receiving antenna at steady state. (Note: the dashed box in (a) and (b) indicate the boundary of the Al/CuO samples, white line in (b) indicates the position of embedded receiving antenna.) (c) Simulation of the near field electric field intensity at the sample position with and without receiving antenna. (d) Temporal temperature profile of the two hot spots. (e) The heating rate of two hot spots (from IR camera video) and electric field intensity (from simulation) at varying source antenna power level.

The simulation indicates that the electric field intensity induced by the embedded receiving antenna increases linearly with source antenna power **(dash line in** Fig. 3**e)**. A general exponential growth relationship between the heating rates and the source antenna power was observed based on Equation (1) **(**Fig. 3**e)**. In the second region we observe a decrease in heating rate. This is presumably because the heat capacity of Al and CuO is increasing with temperature, and the relativity permittivity changes with temperature (Gafner et al., 2015; Havinga, 1961). At longer times, the power input from the receiving antenna is at steady-state with the heat loss from hot spots to the rest of the sample, and a time invariant temperature is achieved.

Since the simulation did not contain Al and CuO nanoparticles or polymer matrix explicitly, it is not possible to calculate theoretical heating rates from the electric field distribution. However, this approach does give a simple estimation of the location of the hot spots induced by the receiving antenna under this complex electric field environment. To confirm this, Al/CuO samples with multiple receiving antennas were fabricated, and compared with simulation results. Two receiving antennas were embedded into the sticks, 10 mm (1/12λ, Fig. 4**(a1)**) and 5 mm (1/24λ, Fig. 4**(b1)**). The IR camera video shows that hot spots are generated at each end of the embedded antennas **(**Fig. 4**(a 2–3) and (b 2–3))**. Comparing the simulation results **(**Fig. 4**(a 4) and (b 4),** Figure S5**)**, clearly electric field gradients were formed at each end of the receiving antennas, the position of these gradients aligned with the position of the hot spots observed from the IR camera. In either case, the induced electric field intensity of the left receiving antenna was less than the right receiving antenna. From the IR camera, the steady state temperature of the left two hot spots is lower than the right two hot spots **(**Fig. 4**a2 and b2)**. Combining the experiment and simulation results, we can conclude that complex heating patterns can be achieved by judicious choice of antenna arrangements.

3.3. *Point and sequential ignition via embedded receiving antenna*

The position of the hot spots was always observed at the terminus of the receiving antenna regardless of their length: from 1/24λ to 1/8λ. Furthermore, increasing the receiving antenna length to 1/6λ (20 mm) and 1/4λ (30 mm), ignition can be triggered **Figure S6** shows simulation results of the induced electric field of 1/6λ and 1/4λ receiving antenna; induced electric field are located at two terminals of the receiving antenna. Fig. 5**(a)** demonstrates the schematic and the color camera imaging of the point ignition with a 1/6λ receiving antenna under 153 W source antenna stimulation. Since the right end of the receiving antenna induces a higher electric field compare to the left end, it is here that ignition first occurs after ~1s. After which a steady flame propagates along the sample in both directions.

With a 1/4λ receiving antenna (Fig. 6**a)** and under the same power stimulation (153 W), the Al/CuO sample was first ignited from the right end, but after 40 to 70 ms, a second ignition was observed at the left end of the receiving antenna, so that two flames propagate toward the sample center. In this way it is possible to have multiple ignition points with one excitation source, and again this implies one can design burn

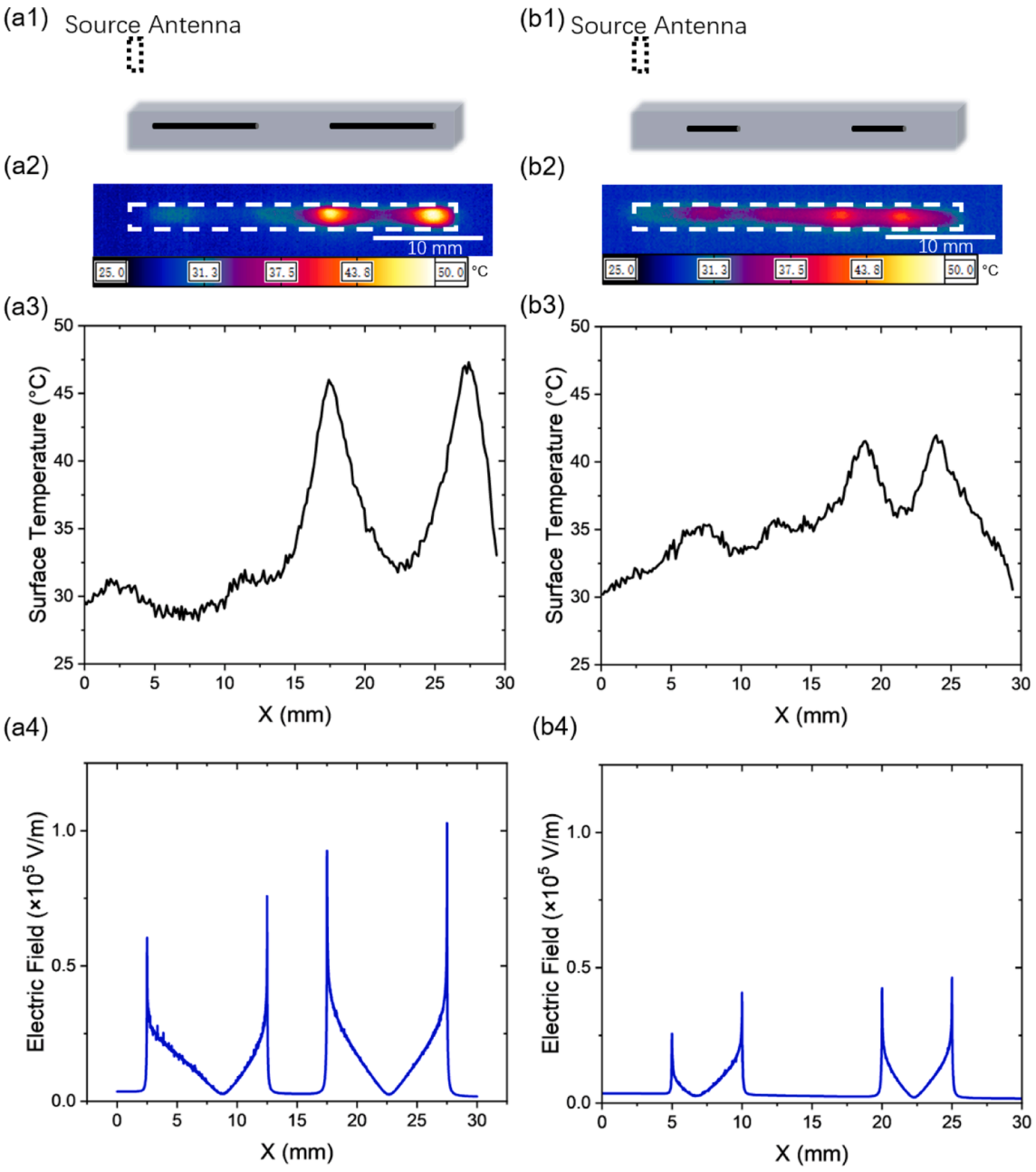

Fig. 4. A1and b1: Al/CuO samples with multiple receiving antennas embedded. a2 and b2: IR camera images of steady state temperature under 76 W MW stimulation (Note: white dash lines indicate boundary of the Al/CuO samples, steady state temperature reached after ~12 s for a2 and ~20 s for b2). a3 and b3: Surface temperature extracted from IR images (a2 and b2). a4 and b4: Simulated electric field distribution along the receiving antennas.

patterns using antennas.

Fig. 5**(b) and 6(b)** show the ignition delay and the heating rate of the right ignition point (right end of the receiving antenna) of the two ignition cases. Both cases show an inverse relationship between the heating rate and ignition delay at the ignition point, suggesting that at below 300 W source antenna power, this is a thermally-limited process (Alibay et al., 2021). Since the heating rate shows an exponential growth with the source antenna power, this indicates that the sample with 1/8λ receiving antenna (Fig. 3) and even shorter receiving antenna (Fig. 4) may also achieve ignition if the monopole source antenna system allows higher power. The 1/4λ receiving antenna shows more efficiency in term of heating rate and ignition delay. This is consistent with the embedded receiving antenna acting as a monopole antenna. According to the classic electromagnetic and transmission line theory, the electrons moving inside the antenna move periodically for a distance of 1/2λ (Kong, 2000). When the length of the dipole antenna also equals 1/2λ, the reflected current from the antenna tip can reinforce with the current from the next cycle. When the length of the embedded receiving antenna, L = 1/4λ, it is equivalent to a 1/2λ dipole antenna, and thus is more efficient compare with 1/6λ and 1/8λ receiving antenna (Chen, 2005).

Another interesting observation is that the ignition with 1/6λ receiving antenna only happened at the right end while there are two ignition points with 1/4λ receiving antenna. The heating rates of the two hot spots from each cases shows that with 1/4λ receiving antenna is higher than the 1/6λ receiving antenna (Fig. 7**a and b)**. However, these heating rate differences is not enough to explain why at each source antenna power level, the 1/6λ receiving antenna sample only has one ignition point. One possible reason is that length of the receiving antenna plays a key role here. In order to achieve ignition via MW

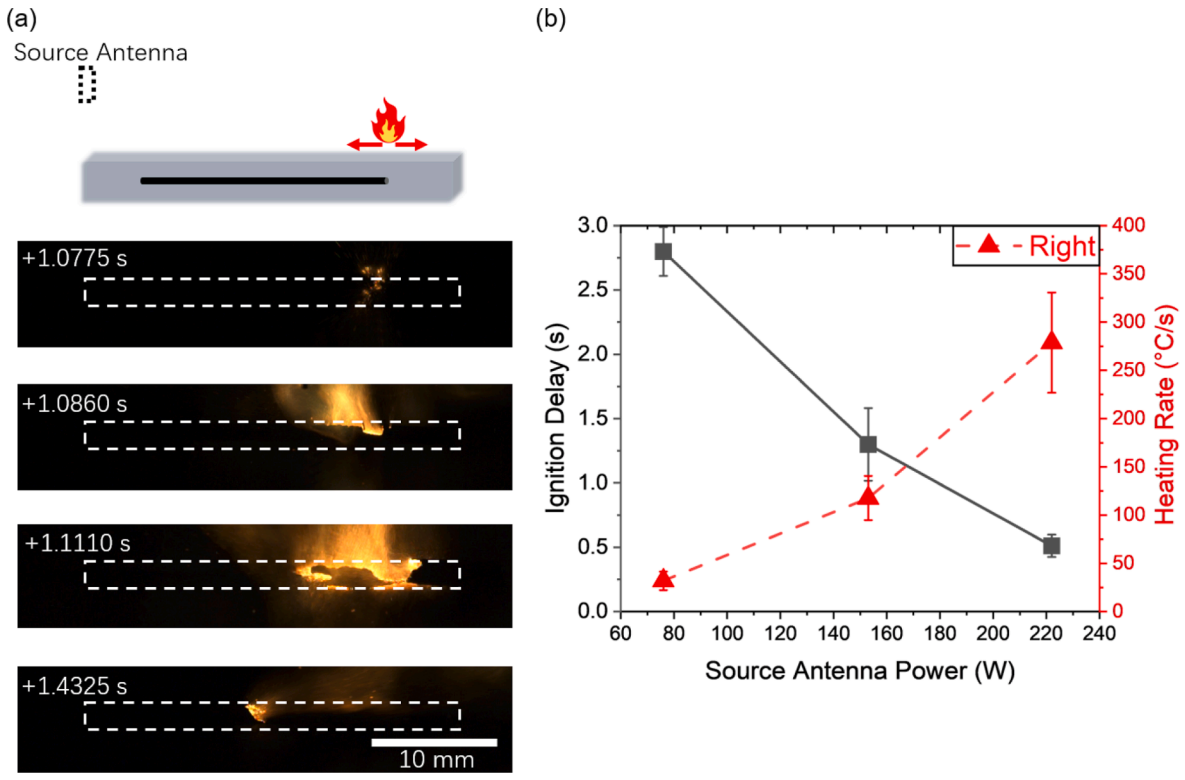

Fig. 5. (a) Select point ignition with 1/6λ receiving antenna. (Note: dash line indicates the sample position.) (b) Heating rate and ignition delay of the ignition point at the location of the right end of the receiving antenna.

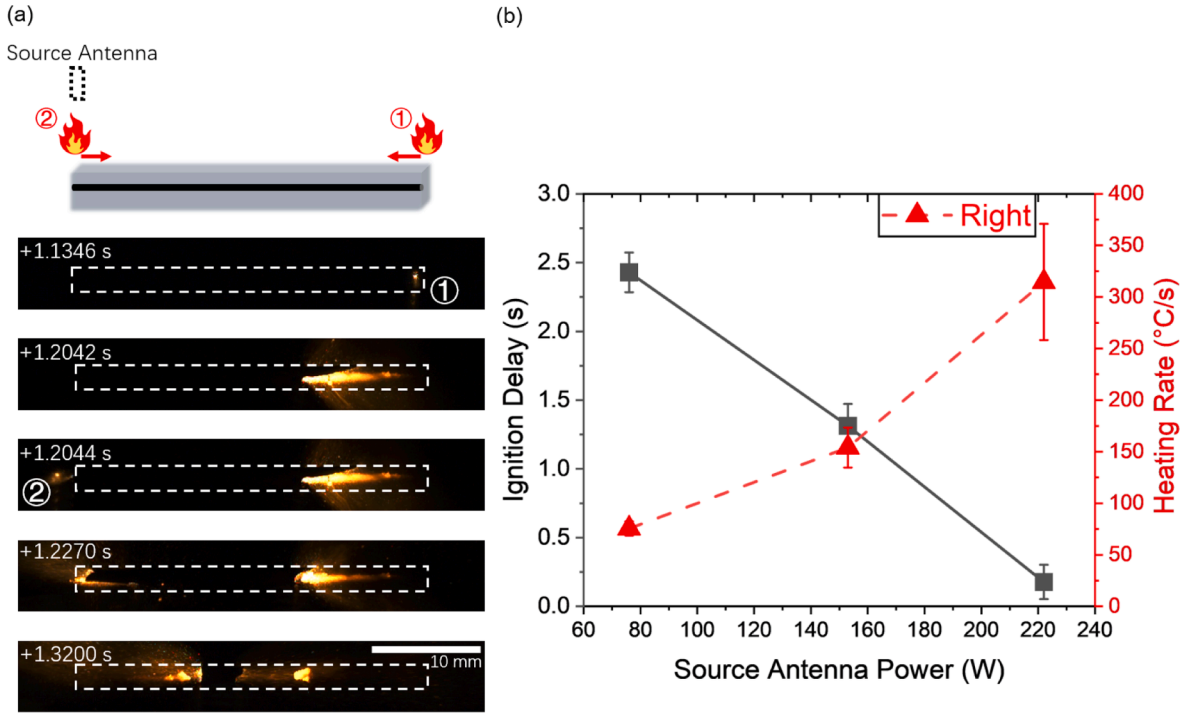

Fig. 6. (a) Sequential two points ignition with 1/4λ receiving antenna. (Note: dash line indicates the sample position, ① and ② indicate the first and second ignition point.) (b) Heating rate and ignition delay of the first ignition point.

stimulation, the energy deposition rate of the Al/CuO composite must exceed the minimum ignition energy (MIE) (Alibay et al., 2022). The length of the receiving antenna controls the heating rate (energy deposition rate) by the induced electric field intensity **(**Fig. 7**c)** (Xie et al., 2009). The embedded Al wires were all consumed after combustion. Considering the flame temperature of the Al/CuO and the melting point of bulk Al, implies the Al wires either melt or reacted during the combustion (Wang et al., 2021). Since the hot spots are generated by the

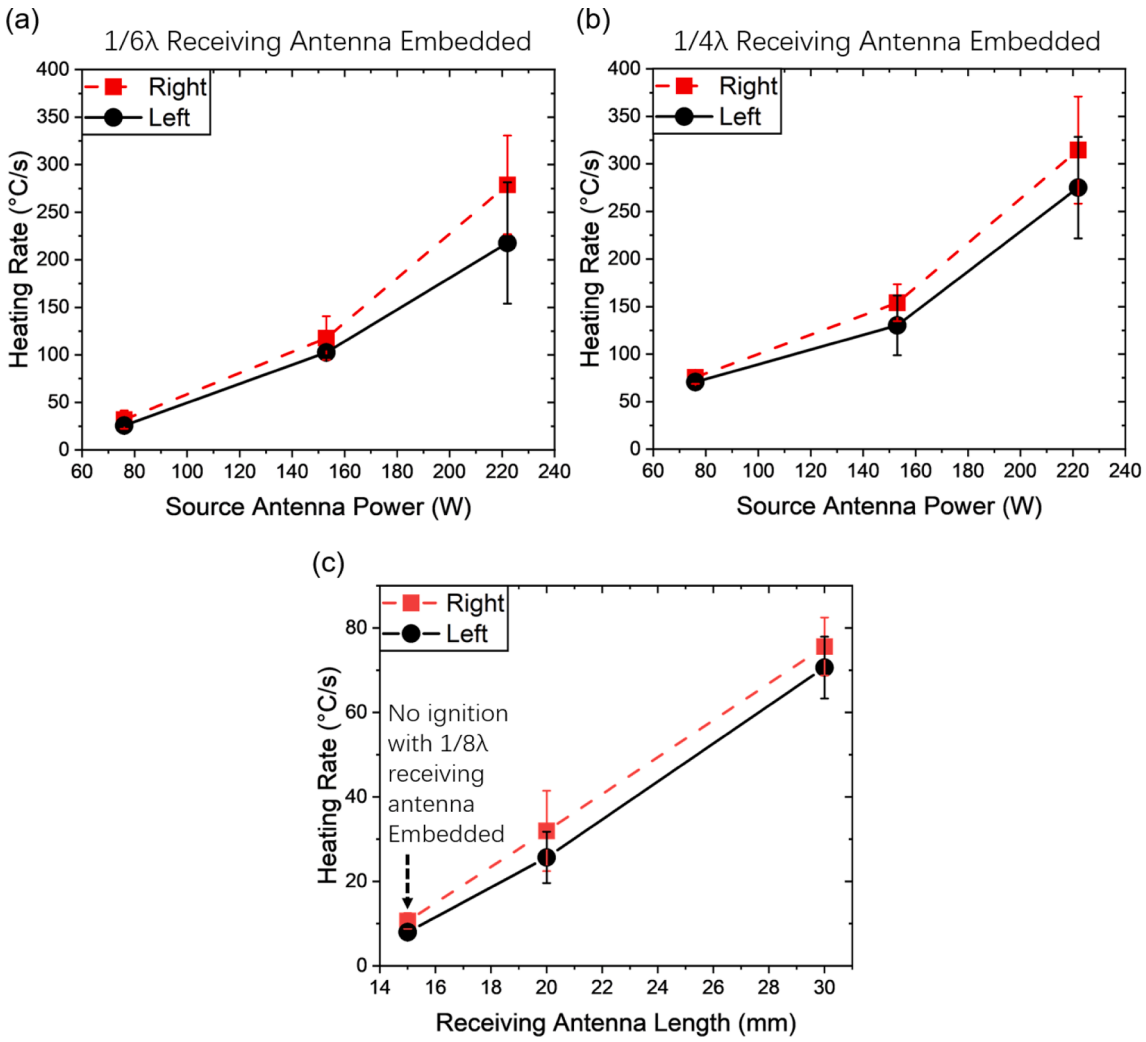

Fig. 7. (a) Measured heating rate of the Al/CuO with 1/6λ receiving antenna. (b) Measured heating rate of the Al/CuO with 1/4λ receiving antenna. (c) Heating rates of the hot spots increasing with embedded receiving antenna length (Source antenna power: 76 W).

induced electric field gradient on the two ends of the receiving antenna, it is possible that with the ignition, the right end of 1/6λ receiving antenna begins melting or reacting. Thus, the total length of the 1/6λ receiving antenna decreases, which also decreases the induced electric field. In the 1/4λ receiving antenna case, the receiving antenna would also decrease following ignition at the right-side ignition point. However, the remaining receiving antenna can still induce sufficient electric field at the left end and trigger a second ignition.

4. Conclusions

In this work, a microwave receiving antenna (Al wire) was embedded into Al/CuO nanothermites via direct writing process. We show that embedding a MW receiving antenna within a printed energetic composite result in focusing of MW energy at the terminals of the receiving antenna (embedded wire) resulting in sufficient heating to induce ignition remotely. It is important to note that the wires themselves do not heat but rather the high induced electric field results in dielectric heating of the sample, and with sufficient electric field strength, trigger ignition. The heating rate of the local hot spots and ignition delay of the embedded sample placed remotely (15 mm) below the monopole source MW antenna were investigated. In all the tested samples with different length of embedded receiving antenna, local hot spots were generated at the ends of the receiving antenna as imaged with an IR camera. Simulation of a monopole source and receiving antennas, shows a spatial correspondence of the calculated electric field and the measured hot spots. By changing the length of embedded receiving antenna, remote ignitions were achieved, and the results are consistent with what might be expected based on classical antenna theory. We also demonstrate that receiving antennas can be incorporated to trigger ignition in desired locations, with multiple ignition points from which flame propagations can be induced. This study provides a new way to design and remote control the location of the hot spots and ignition by embedding receiving antenna into non-MW sensitive composites.

Declaration of Competing Interest

The authors declare that they have no known competing financial interests or personal relationships that could have appeared to influence the work reported in this paper.

Data availability

Data will be made available on request.

Acknowledgements

The authors gratefully acknowledge support from the Air Force Office of the Scientific Research (AFOSR) Multidisciplinary University Research Initiative (MURI) program on piezoenergetic materials. The

authors thank the CFAMM at UC Riverside for electron microscopy support. The authors also thank Qiran Wu and Prof. Yongtao Cui for help with the Vector Network Analyzer.

Appendix A. Supplementary data

Supplementary data to this article can be found online at https://doi.org/10.1016/j.ces.2023.118948.

References:

Alibay, Z., Kline, D.J., Rehwoldt, M.C., Biswas, P., Herrera, S., Wang, H., Zachariah, M. R., 2021. Mechanism of microwave-initiated ignition of sensitized energetic nanocomposites. Chem. Eng. J. 415, 128657 https://doi.org/10.1016/j.cej.2021.128657.

Alibay, Z., Olsen, D., Biswas, P., England, C., Xu, F., Ghildiyal, P., Zhou, M., Zachariah, M.R., 2022. Microwave stimulation of energetic Al-based nanoparticle composites for ignition modulation. ACS Appl. Nano Mater. 5, 2460–2469. https://doi.org/10.1021/acsanm.1c04157.

Asay, B.W., Son, S.F., Busse, J.R., Oschwald, D.M., 2004. Ignition characteristics of metastable intermolecular composites. Propellants Explos. Pyrotech. 29, 216–219. https://doi.org/10.1002/prep.200400049.

Barkley, S.J., Lawrence, A.R., Zohair, M., Smithhisler, O.L., Pint, C.L., Michael, J.B., Sippel, T.R., 2021. Smart electromagnetic thermites: GO/rGO nanoscale thermite composites with thermally switchable microwave ignitability. ACS Appl. Mater. Interfaces 13, 39678–39688. https://doi.org/10.1021/acsami.1c04476.

Biswas, P., Mulholland, G.W., Rehwoldt, M.C., Kline, D.J., Zachariah, M.R., 2020. Microwave absorption by small dielectric and semi-conductor coated metal particles. J. Quant. Spectrosc. Radiat. Transf. 247, 106938 https://doi.org/10.1016/j.jqsrt.2020.106938.

Chen, W.-K., 2005. The Electrical Engineering Handbook. Elsevier Academic Press, Amsterdam.

Cheng, J., Zhang, Z., Wang, Y., Li, F., Cao, J., Gozin, M., Ye, Y., Shen, R., 2022. A smart thermite with tunable properties – doping of Al/Cuo with microwave absorbing Ti3c2 Mxene for improved ignition and combustion performance. SSRN Journal. https://doi.org/10.2139/ssrn.4123907.

Crane, C.A., Pantoya, M.L., Weeks, B.L., 2014. Investigating the trade-offs of microwave susceptors in energetic composites: microwave heating versus combustion performance. J. Appl. Phys. 115 (10), 104106 https://doi.org/10.1063/1.4868337.

Field, J.E., 1992. Hot spot ignition mechanisms for explosives. Acc. Chem. Res. 25, 489–496. https://doi.org/10.1021/ar00023a002.

Gabriel, C., Gabriel, S., H. Grant, E., H. Grant, E., S. J. Halstead, B., Michael P. Mingos, D., 1998. Dielectric parameters relevant to microwave dielectric heating. Chem. Soc. Rev. 27 (3), 213.

Gafner, Y.Y., Gafner, S.L., Zamulin, I.S., Redel, L.V., Baidyshev, V.S., 2015. Analysis of the heat capacity of nanoclusters of FCC metals on the example of Al, Ni, Cu, Pd, and Au. Phys. Metals Metallogr. 116 (6), 568–575.

Granier, J.J., Pantoya, M.L., 2004. Laser ignition of nanocomposite thermites. Combust. Flame 138, 373–383. https://doi.org/10.1016/j.combustflame.2004.05.006.

Havinga, E.E., 1961. The temperature dependence of dielectric constants. J. Phys. Chem. Solid 18, 253–255. https://doi.org/10.1016/0022-3697(61)90169-X.

Himmetoglu, B., Wentzcovitch, R.M., Cococcioni, M., 2011. First-principles study of electronic and structural properties of CuO. Phys. Rev. B 84, 115108. https://doi.org/10.1103/PhysRevB.84.115108.

Kline, D.J., Rehwoldt, M.C., Turner, C.J., Biswas, P., Mulholland, G.W., McDonnell, S.M., Zachariah, M.R., 2020. Spatially focused microwave ignition of metallized energetic materials. J. Appl. Phys. 127 (5), 055901 https://doi.org/10.1063/1.5134089.

Kong, J.A., 2000. Electromagnetic wave theory. EMW Publishing, Cambridge, MA.

Vargas, E., Pantoya, M.L., Saed, M.A., Weeks, B.L., 2016. Advanced susceptors for microwave heating of energetic materials. Mater. Des. 90, 47–53. https://doi.org/10.1016/j.matdes.2015.10.110.

Wang, H., Jian, G., Egan, G.C., Zachariah, M.R., 2014. Assembly and reactive properties of Al/CuO based nanothermite microparticles. Combust. Flame 161, 2203–2208. https://doi.org/10.1016/j.combustflame.2014.02.003.

Wang, H., Kline, D.J., Rehwoldt, M.C., Zachariah, M.R., 2021. Carbon fibers enhance the propagation of high loading nanothermites. in situ observation of microscopic combustion. ACS Appl. Mater. Interfaces 13, 30504–30511. https://doi.org/10.1021/acsami.1c02911.

Wang, Q.J., Wang, J.B., Zhong, X.L., Tan, Q.H., Hu, Z., Zhou, Y.C., 2012. Magnetism mechanism in ZnO and ZnO doped with nonmagnetic elements X (X = Li, Mg, and Al): a first-principles study. Appl. Phys. Lett. 100, 132407 https://doi.org/10.1063/1.3698096.

Williams, R.A., Beloni, E., Dreizin, E.L., 2012. Ignition of metal powder layers of different thickness by electrostatic discharge. J. Propul. Power 28, 132–139. https://doi.org/10.2514/1.B34231.

Xie, H., Kong, F.M., Li, K., 2009. The electric field enhancement and resonance in optical antenna composed of AU nanoparicles. Journal of Electromagnetic Waves and Applications 23, 534–547. https://doi.org/10.1163/156939309787612419.